

**PAPER**

Heaping and secondary flows in sheared granular materials

David Fischer¹, Tamás Börzsönyi², Daniel S Nasato³, Thorsten Pöschel³ and Ralf Stannarius¹¹ Institute of Experimental Physics, Otto von Guericke University, Universitätsplatz 2, D-39106 Magdeburg, Germany² Institute for Solid State Physics and Optics, Wigner Research Center for Physics, Hungarian Academy of Sciences, PO Box 49, H-1525 Budapest, Hungary³ Institute for Multiscale Simulation, Friedrich-Alexander-Universität Erlangen-Nürnberg, Nögelsbachstr. 49 b, D-91052 Erlangen, GermanyE-mail: ralf.stannarius@ovgu.de**Keywords:** granular material, shear flow, split-bottom geometry, secondary flow**OPEN ACCESS****RECEIVED**

29 February 2016

REVISED

22 September 2016

ACCEPTED FOR PUBLICATION

11 October 2016

PUBLISHED

4 November 2016

Original content from this work may be used under the terms of the [Creative Commons Attribution 3.0 licence](https://creativecommons.org/licenses/by/4.0/).

Any further distribution of this work must maintain attribution to the author(s) and the title of the work, journal citation and DOI.

**Abstract**

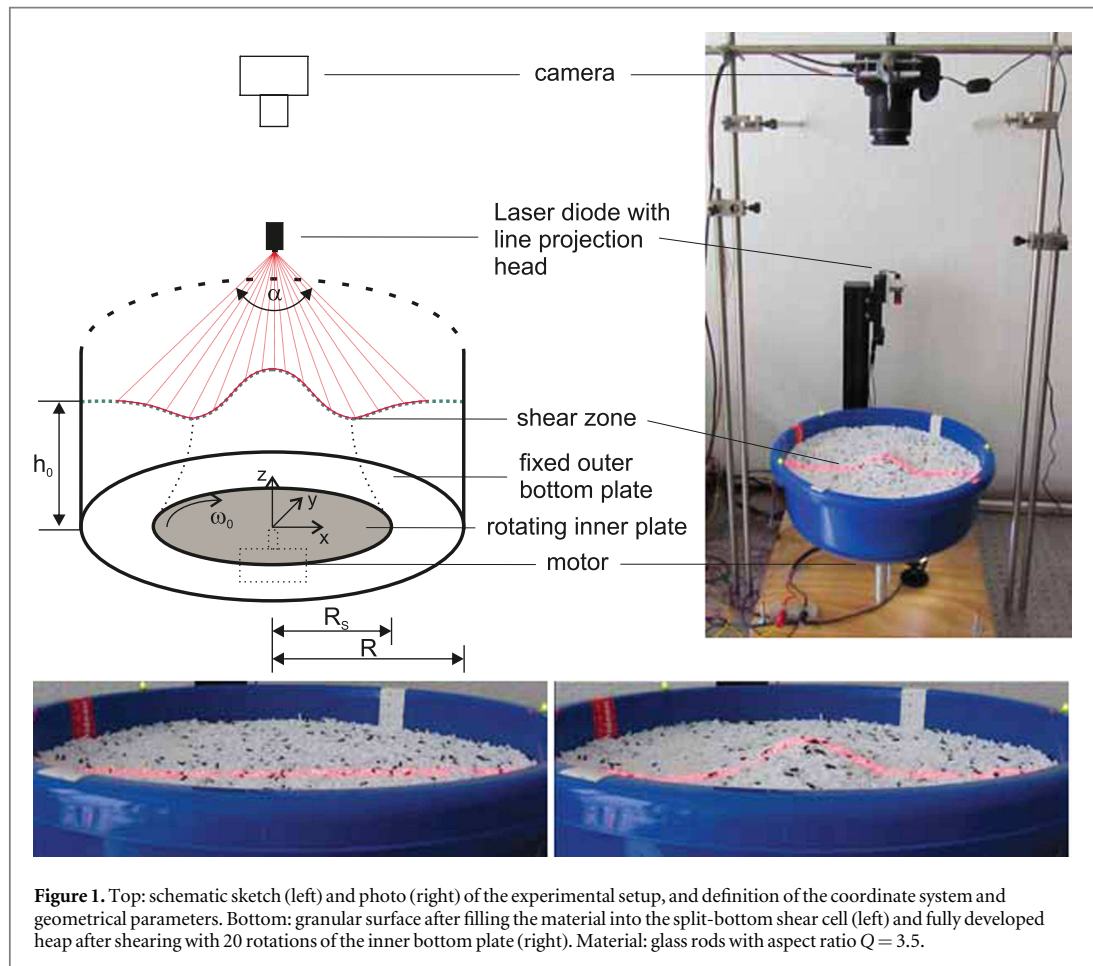
Cylindrical containers with a rotating bottom disk (so-called split-bottom geometry) are well established devices to shear granular materials in a continuous way, and to generate well-defined localized shear bands in the granular bed. When material composed of shape-anisotropic grains is sheared in such a container, a secondary flow is generated that leads to the formation of a considerable heap of material near the rotation center. We demonstrate that this effect can be found not only with prolate grains, as shown in a previous study, but also for oblate particle shapes. In addition, the quantitative influence of geometric and dynamic parameters is studied systematically. It is shown that the fill height of the container has considerable influence on the time scale for heap formation, but much less effect on the heap height. Results of numerical simulations agree with the experimental findings and provide insight in the particle dynamics.

1. Introduction

Flow in granular material is a ubiquitous phenomenon, shaping landscapes, ruling the transport and processing of numerous agricultural goods, and influencing technological processes e.g. in the mining and building industries. It is involved in everyday life when we pour cereals or rice in a bowl, fill salt shakers or a popcorn bag, or when a hole is dug in the garden. The processing of granular material has thus been a common task since earliest ages of human history. But nevertheless, flowing granulate still holds lots of mysteries for scientists, and its satisfactory description is far from being achieved. One of these unconventional phenomena that has been described only recently is the heaping of elongated cylindrical and ellipsoidal particles that are sheared in a cylindrical geometry [1]. Other topical problems are related, e.g. to the phenomena of jamming [2–4], clogging [5, 6] and orientational alignment of shape-anisotropic grains [7, 8].

A useful introduction into the topic of granular dynamics can be found in reviews (e.g. [9–11]). Peculiarities of shape-anisotropic granular matter have been compiled in a recent review [12]. There, an overview of the specific packing problems, shear flow, alignment and orientational order of these materials is given and relevant literature is collected.

One of the standard geometries for the investigation of continuous shear flow in granular material is the cylindrical container with split bottom [13–15]. The central part of the bottom plate can be rotated with respect to the outer border. It has been employed to investigate, e.g. shear zone geometries [16–18], dilatancy and packing [19–21], segregation [22, 23], alignment and orientational order [7, 24, 25], macroscopic viscosities [26, 27] and secondary flows [1, 28]. The latter was also reported for a slightly different Taylor–Couette geometry [29]. Wortel *et al* [1] described the following characteristic properties of elongated grains under shear in split-bottom containers: the material formed a heap in the central region, which reached a saturation height after some transient phase. When the rotation sense was reversed, the heap first collapsed, then reformed at the same time scale as the initial transient. Heaping was found only in a certain range of fill levels of the container. No significant heaps were reported for high and low container fill heights, where the central part of the granular bed



surface stays at rest or rotates synchronously with the bottom disk, respectively. At intermediate fill heights, the surface grains above the bottom disk rotate at a reduced rate, producing a substantial secondary flow. Then, the heap elevation is maximal.

After removal of the heap material and continued shearing, the heap rebuilds again. At each reversal of the shear direction, the heap collapses and reappears again afterwards. However, data for rice grains were difficult to reproduce quantitatively in individual experiments. Preliminary work included also a qualitative interpretation of the effect on the basis of symmetry arguments.

In this study, a comprehensive quantitative analysis of flow processes and heaping in the split-bottom geometry is presented. We avoided using rice grains as in [1] since quantitative reproducibility of the effect with this material is not satisfactory. The previous work is extended by numerical simulations which reveal the particle arrangement and dynamics in the bulk. We relate the heap geometry with the primary and secondary flow dynamics in the granulate. The behavior of prolate, oblate and isotropically shaped grains is investigated and compared. Geometrical parameters (fill height of the container), dynamic parameters (shear velocity), and material parameters are systematically varied, and transients after initiation of shear, and the reversal of shear are analyzed.

2. Experimental

2.1. Setup and materials

The experimental setup is sketched in figure 1, top. A rotationally symmetric (nearly cylindrical) bowl is mounted on a table such that the inner bottom disk can be rotated by a motor with defined angular velocities. The rotating bottom plate has a radius $R_s = 118$ mm and the stationary outer boundary has a radius of $R = 175$ mm. Friction between the bottom and the granular layer is increased by sand paper glued to all bottom parts. Rotation of the central plate is driven by a 12 V DC motor, controlled by an *Arduino UNO* microcontroller with a *LabVIEW*-program. Both the direction of rotation and different rotation speeds ω_0 can be chosen.

Table 1. Lengths ℓ , diameters d and aspect ratios Q of the investigated grains. Photos show the individual grains at comparable scales.

	Peas	Airsoft bullets	Wooden pegs			Glass rods	Lentils	
								
ℓ (mm)	—	—	10	20	25	40	6.6	≈ 2.5
d (mm)	≈ 7	6	5	6	5	5	1.9	≈ 7.0
Q	1	1	2	3.3	5	8	3.5	0.36

Initially, the granulate is filled into the container up to a height h_0 , and carefully leveled. Fill heights are varied between 30 and 100 mm. The contactless measurement of the granular bed surface is achieved with a Laser ($\lambda_{\text{Laser}} = 635$ nm) in combination with a cylinder lens (beam expansion angle $\alpha = 80^\circ$). The laser line is directed onto the granular surface at an angle of 45° . The surface profiles are recorded with a commercial digital camera *Canon EOS 600D*, with an image resolution of 8 pixel/mm at a maximum frame rate of 2 frames s^{-1} . For the tracking of individual particles at the granular surface, additional video sequences with a resolution of 3 pixel/mm and a rate of 30 frames s^{-1} are recorded. The camera view is vertical to the initial granular surface. The deflection of the laser line on the elevated surface allows to monitor the heap profile in a cross section containing the rotation axis. In the above described geometry, the laser sheet produces a straight line on a flat surface. Any elevation of the surface shifts the projection of this line in the camera image by a distance proportional to the height of the elevation. The method relies on the condition that the lateral extension of the heap is large compared to the elevation, which is clearly fulfilled in the experiments. We assume that the mean heap profile has rotational symmetry about the rotation axis, thus the deflection of the line provides all relevant information on the heap shape. Both the instant images and the video sequences can be recorded with the camera. The evaluation of the optical images is performed by means of *Matlab* software.

The materials chosen for the shear experiments are listed in table 1. One part is a set of wooden pegs with different lengths to explore the influence of the aspect ratio. Glass rods have a comparable aspect ratio to one of the wooden pegs, but much smaller sizes. In addition, we study lentils as representatives of oblate grains. Peas (nearly spherical shapes and a few percent polydispersity) as well as airsoft balls (perfect smooth spherical surface, monodisperse) serve for the comparison with isotropically shaped grains. For a qualitative visualization and quantitative analysis of the secondary flow, some of the grains have been colored as tracer particles. We refrained here from the investigation of rice grains as in Wortel's experiments [1], because they give less reproducible results, particularly for the heap heights, but also for the heap growth dynamics.

In figure 1, bottom, the shear cell is shown immediately after preparation (left) and after the first 20 revolutions of the bottom disk (right). It is filled with glass rods of length $\ell = 6.6$ mm, and diameter $d = 1.9$ mm. The red line clearly visualizes the emerging heap, which lifted the granular surface in the center of the shear cell by approximately 30% compared to the initial fill height $h_0 = 80$ mm.

2.2. Data analysis

The surface profiles are evaluated with a *Matlab* program. The position of the laser line $y(x)$ (figure 1, bottom) is determined and yields the height profile $h(r)$. Height profiles were averaged over 1 mm steps, which is less than the particle dimensions. Thus, details in the height profile smaller than particle sizes appear as arbitrary fluctuations of the height profiles, which can be averaged when multiple images are compared. We define the heap height h_{max} as the (maximum) elevation of the grain bed at the center ($r = 0$), respective to the initial fill height.

The packing density of the granulate changes during the shearing process, Reynolds dilatancy competes with alignment effects and spatial ordering [21]. We evaluate the global packing density by measurement of the total granular volume. Again, rotational symmetry is assumed and the laser line is evaluated to give the local bed height. At each time step t , we sum volumes of cylindrical shells with radii $r_i - r_{i-1}$ and heights $h(r_i)$ to approximate the total volume

$$V(t) = \sum_i V_i(t) = \sum_i \pi (r_i - r_{i-1})^2 \cdot h(r_i). \quad (1)$$

The step width for r_i from the digitized laser contour is 1 mm. In the plots of volume data we present $V(t)$ normalized with the initial volume $V_0 = \pi R^2 h_0$.

2.3. Direct visualization of secondary flow

Particle motion towards the granular surface is demonstrated in a first, qualitative experiment with $Q = 5$ wooden pegs. For that purpose, colored pegs were prepared in three vertical layers in distances of 20 mm between each other (figure 2). Each layer contains 90 pegs with colors green, blue, red (from top to bottom).

A heap was clearly visible five bottom plate revolutions after the rotation was started ($\omega_0 = 10$ rpm). Concurrently after about five revolutions, the first layer of colored pegs reached the surface of the granular bed, evidencing an upstream in the axial center of the container. In accordance with the preparation, green, blue and red pegs emerged in approximately equal intervals. From there, a radial displacement of colored grains downhill towards the shear zone was observed. Within the shear zone, the tracer particles submerge again. Figure 2 shows the granular surface in this experiment at different instants during the shearing.

After 100 revolutions, the experiment was stopped and the granulate was excavated layer by layer. Results of this excavation are depicted in figure 3. It is evident that the colored pegs have moved in vertical direction, some of them upward, others downward, all three colors were present in each excavation slice. In radial direction, the range with colored pegs expanded about 2.5 times from 100 to 250 mm.

The trajectories of individual pegs can be monitored when only few tracers are used. Figure 4 left depicts the radial distance r from the rotation axis for a single particle. A directed motion from the center towards the shear zone is evident. The shear zone extends in the range from 60 to 120 mm. After about 20 revolutions, the particle was temporarily trapped in the shear zone, then it submerged out of sight into deeper layers, to reappear after about 40 rotations near the container axis. This trajectory is a direct hint on a convection cell in the granular bed, and it provides a crude estimate for the velocity of this convective stream.

For a determination of particle velocities we add approximately 10% colored particles which are otherwise identical with the uncolored material. These are extracted from the images with a color recognition program and their positions are assembled to trajectories. By averaging all detected particles in each radial 5 mm zone, the angular velocity of the primary flow at the surface, $\omega(r) = \Delta\phi/\Delta t$, can be determined. In addition, the radial velocity profile $v(r) = \Delta r/\Delta t$ is extracted, which yields information on the secondary flow on the granular bed surface (figure 4, left). Here, positive velocities correspond to an outward motion of the grains.

Even though this experiment provides only information on particle displacements on the granular surface and flow in deeper layers cannot be seen directly, it is evident that over a period of 50 bottom disk rotations the traced particle moved back a distance of about 80 millimeters before it reappeared near the center of the container at the heap. This makes clear that the secondary flow has the form of a closed cycle as already suggested in [1]. The particle's outward velocity at the granular bed surface is faster than the inward motion in the lower layers. From 10 independent experiments, a mean radial velocity of $3.0 \text{ mm revolution}^{-1}$ towards the shear zone was found. Thus, the secondary flow in the convection roll is approximately two orders of magnitude slower than the primary flow. It is also evident from the exemplary trajectory of figure 4, and confirmed in other tracks that were evaluated, that the particle displacement proceeds more or less continuous, thus no avalanche drives the particle downhill (this would be reflected in a stepwise graph of $r(\omega t)$ in the figure). Such avalanches are occasionally observed [1], but apparently they do not provide the major contribution to the secondary flow.

2.4. Numerical simulations

The heap formation in the cylindrical split-bottom geometry was also investigated through numerical simulations using the discrete element method (DEM) [30] as simulation tool. DEM is a particle-based method which accounts for the physical model of interparticle forces as well as considers the geometric shape of the particles [31, 32]. Particle-particle and particle-wall interactions were calculated using a normal and a tangential component with an elastic (spring) and a viscous (damping) term. When two spherical particles i and j with radii R_i and R_j , respectively, are in contact, they interact and are allowed to slightly overlap or deform. This overlap can be written in the form [33]:

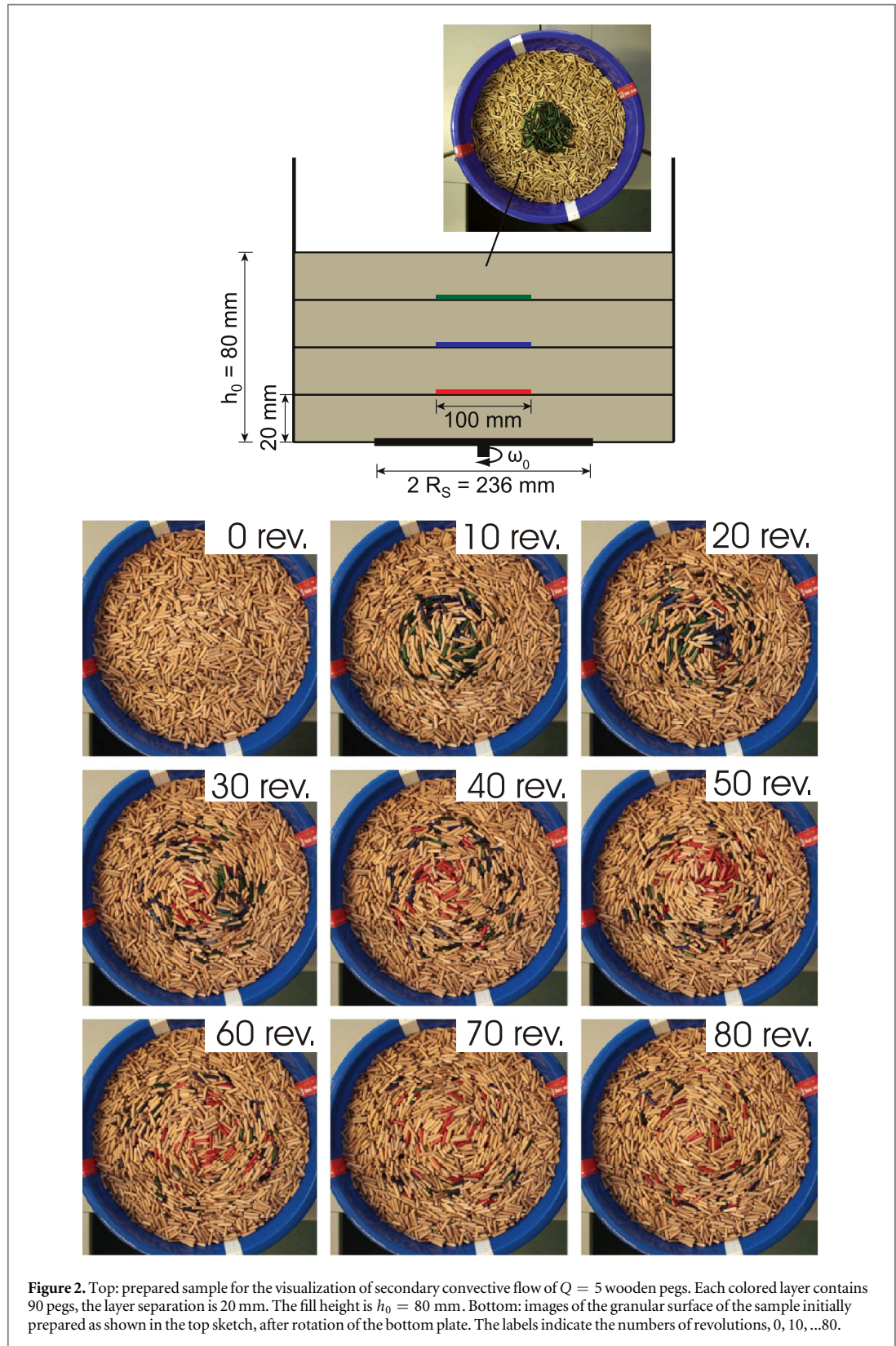
$$\xi = R_i + R_j - |r_i - r_j|, \quad (2)$$

where r_i and r_j are the positions of particle i and j , respectively. Particles are purely elastic (no plastic deformation), i.e. after separation of the contacting particles they recover their initial shape. Normal and tangential spring/damping system can be written in the form:

$$m^* \ddot{\xi} = (k_n \xi_n + c_n \dot{\xi}_n) + (k_t \xi_t + c_t \dot{\xi}_t) \quad (3)$$

with k_n , k_t the normal and tangential elastic parameter, and c_n and c_t the normal and tangential viscous parameters. m^* is the equivalent mass calculated from $1/m^* = 1/m_i + 1/m_j$. No adhesive force is assumed in our models, and the elastic and viscous parameters are given by the Hertz-Mindlin [34] model in the form:

$$k_n = \frac{4}{3} Y^* \sqrt{R^* \xi_n} \quad c_n = -2 \sqrt{\frac{5}{6}} \beta \sqrt{S_n m^*} \geq 0, \quad (4)$$



$$k_t = 8G^* \sqrt{R^* \xi_n} \quad c_t = -2 \sqrt{\frac{5}{6}} \beta \sqrt{S_t m^*} \geq 0 \quad (5)$$

with R^* being the equivalent radius obtained from $1/R^* = 1/R_i + 1/R_j$. Parameters S_n , S_t and β are obtained from:

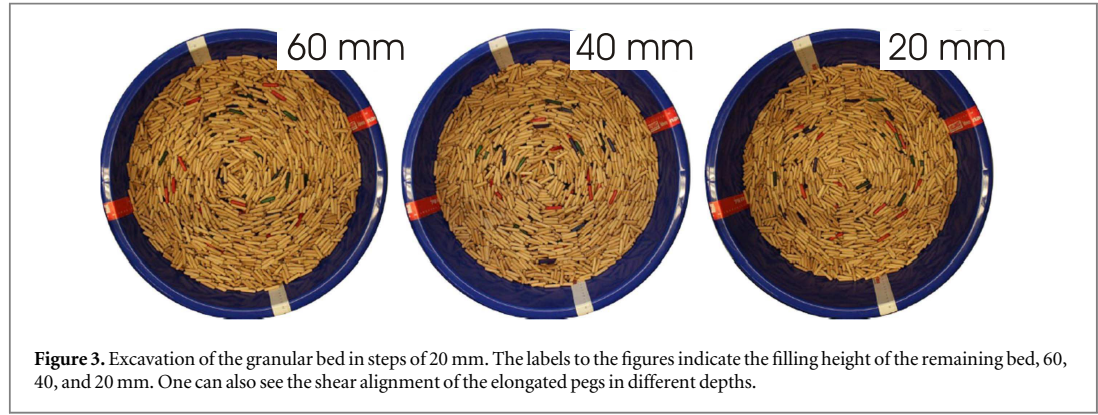


Figure 3. Excavation of the granular bed in steps of 20 mm. The labels to the figures indicate the filling height of the remaining bed, 60, 40, and 20 mm. One can also see the shear alignment of the elongated pegs in different depths.

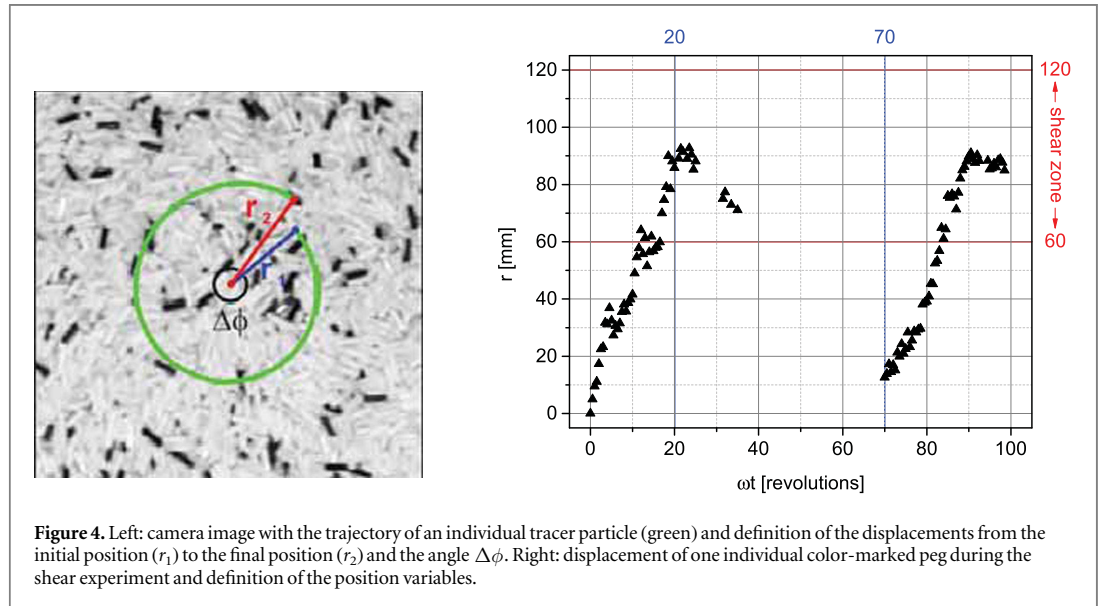


Figure 4. Left: camera image with the trajectory of an individual tracer particle (green) and definition of the displacements from the initial position (r_1) to the final position (r_2) and the angle $\Delta\phi$. Right: displacement of one individual color-marked peg during the shear experiment and definition of the position variables.

$$S_n = 2Y^* \sqrt{R^* \xi_n} \quad S_t = 8G^* \sqrt{R^* \xi_n} \quad \beta = \frac{\ln(e)}{\sqrt{\ln^2(e) + \pi^2}}, \quad (6)$$

where e is the coefficient of restitution, Y^* the equivalent Young's modulus obtained from $1/Y^* = (1 - \nu_i^2)/Y_i + (1 - \nu_j^2)/Y_j$ and G^* the equivalent shear modulus obtained from $1/G^* = 1 - \nu_i^2/G_i + (1 - \nu_j^2)/G_j$.

The tangential part of the viscoelastic force is divided in a shear (elastic) and dissipative part. The shear force is responsible for applying a torque to the particles and is calculated as a history effect between the particles for the duration of the time they are in contact. It is calculated by adding up the relative tangential velocity at the contact point times the time-step size.

The coefficient of friction μ_s is the upper limit of the tangential force through the Coulomb criterion $F_t = \mu_s F_n$, where F_t and F_n are the tangential spring and total normal force components. Thus the tangential force between particles grows according to the previously described force model until $F_t/F_n = \mu_s$ and is then held at $F_t = \mu_s F_n$ until the particles lose contact. The tangential damping contribution is only added in time-steps where there is no slip, i.e. the Coulomb criterion is not met. For a more detailed description we refer to [34].

Simulations were performed using three different materials. In the first case, a purely spherical model was used to represent the experiments with peas. In the second and third cases, wooden pegs and glass rods were modeled as agglomerated spheres—known as clump representation [35, 36]—to capture the geometry and aspect ratio of real particles. Contact detection and force calculation are done on a sphere base as previously described. To avoid double calculation of overlapped regions in the inertial properties, the center of mass and moment of inertia are calculated numerically using a Monte Carlo method. Inertial properties are then used in a

Table 2. Lengths ℓ , diameters d , aspect ratios Q and number of spheres of the particle models used in the DEM simulations. Images show the individual particles at comparable scales.

	Peas	Wooden pegs	Glass rods
			
ℓ (mm)	—	25	6.6
d (mm)	≈ 7	5	1.9
Q	1	5	3.5
N (spheres)	1	11	5

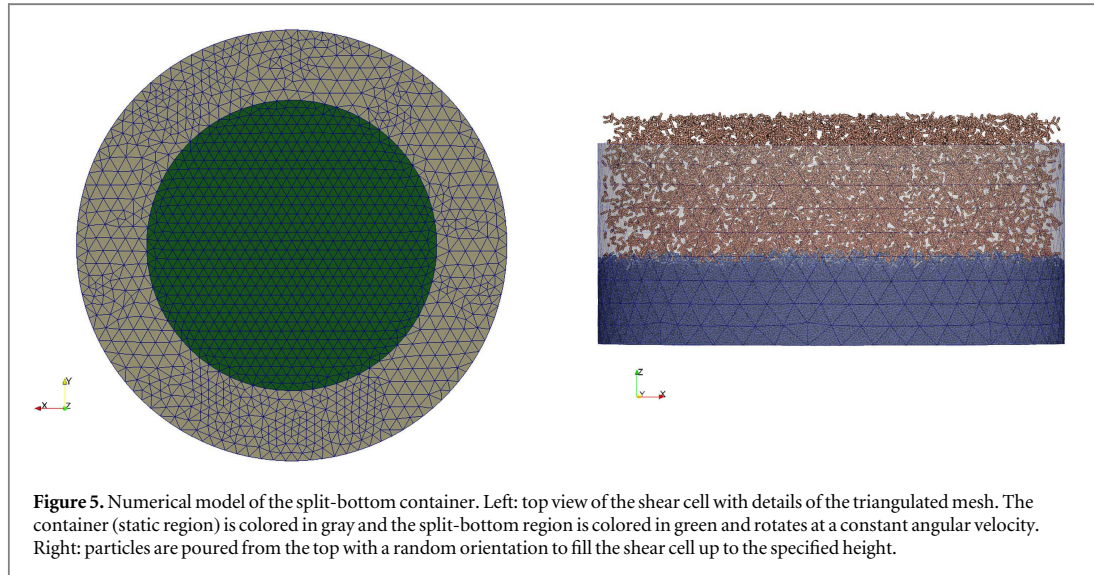


Table 3. Material parameters used in numerical simulations.

Parameter	Peas	Wooden pegs	Glass rods
Material density (kg m^{-3})	1100	850	2500
Young's modulus (Pa)	$5.0\text{E} + 07$	$5.0\text{E} + 07$	$5.0\text{E} + 07$
Poisson's ratio	0.40	0.35	0.35

rotation matrix [32] and the particles are allowed to rotate as rigid bodies due to the torque originated from the tangential forces.

Wooden pegs were modeled by using 11 overlapping spheres clumped together. However for the glass rods only five spheres were used due to the large simulation size, 1.34 million spheres. Further refinements in terms of number of spheres would significantly increase the simulation time. Representations of the particles used in the numerical simulations are sketched in table 2.

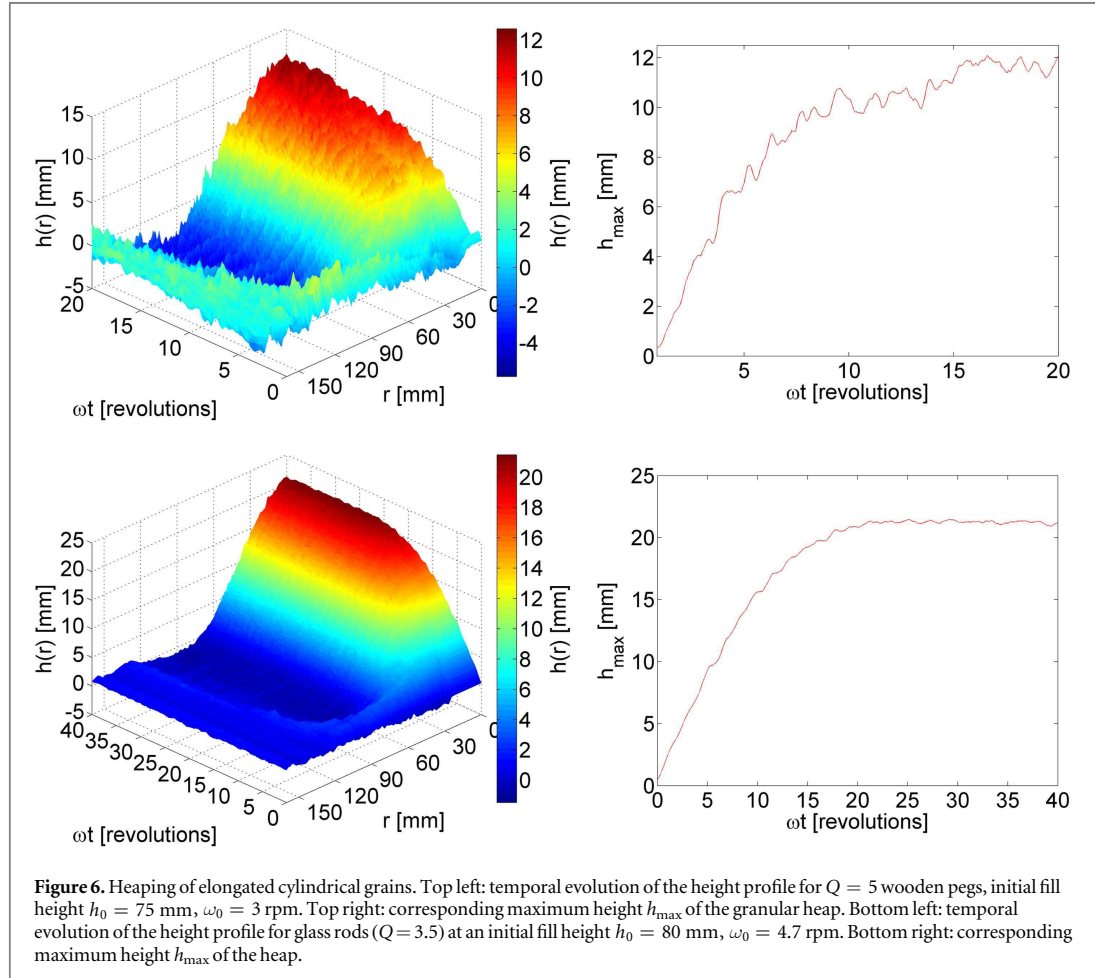
The cylindrical container was modeled as rigid walls and discretized as a triangulated mesh. The split-bottom region was modeled as a separated mesh to allow it rotate independently of the container. The same dimensions used in the experimental setup were also used in the container mesh model.

Particles are poured from the top with random orientation and allowed to settle down before the shearing process starts. The same model used for particle–particle was adopted for particle–wall interactions. Details of the pouring process are shown in figure 5.

Material properties adopted in the numerical simulations are described in table 3. Note that the particle material density is consistent with the one for real materials, but the Young's modulus used in the simulations is smaller than the real value (about 50 GPa for glass). This is because the computational time required for a DEM

Table 4. Interaction parameters used in the contact models and adopted in our numerical simulations.

Parameter	Peas–peas	Peas–wall	Pegs–pegs	Pegs–wall	Rods–rods	Rods–wall
Coeff. of friction	0.30	0.75	0.30	0.75	0.75	0.75
Coeff. of restitution	0.35	0.45	0.30	0.50	0.70	0.65



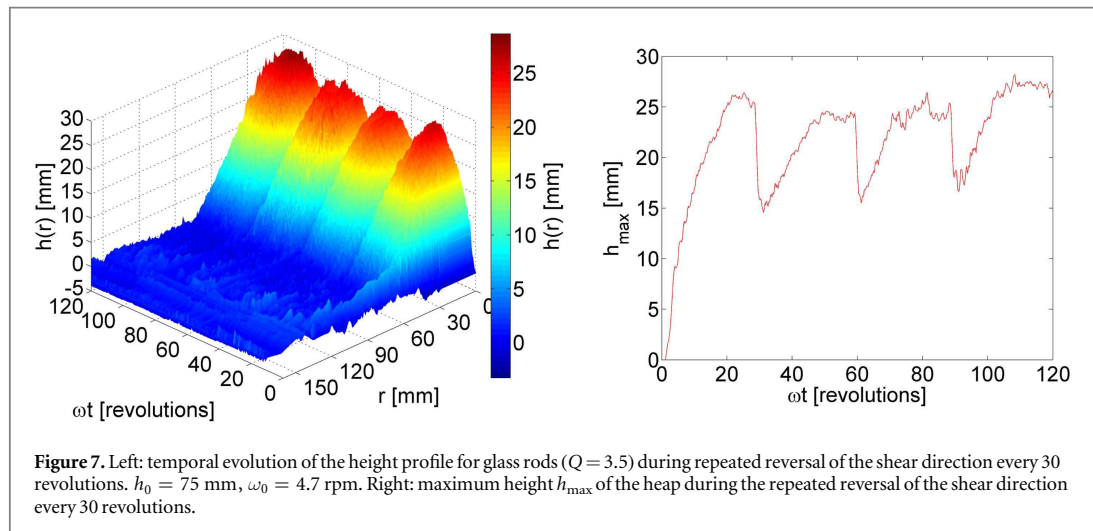
simulation decreases with the reduction in the value of the Young's modulus—the numerical solution remains stable with a larger time step by Rayleigh criteria [37]. Interaction parameters necessary for the contact model between particles and particle-mesh (wall) are described in table 4.

3. Experimental results

3.1. Heap formation and critical parameters

In the following, we analyze the conditions for the formation of a granular heap under cylindrical shear. Experiments with isotropic objects like peas or airsoft balls do neither show a systematic radial flow nor noticeable heaping. The corresponding data are shown in the [appendix](#). The absence of heaping for isotropic grain shapes has been mentioned before [1]. First, we describe results for prolate particles with aspect ratios between 2 and 8. Then, we extend the experiments to oblate particle shapes. In both cases, heaps are observed.

As described above, the displacement of the Laser line on the granular surface is converted into the local height profile $h(r)$. Then, sequences of these profiles are stacked to space–time plots. An example is shown in figure 6, top left, in the form of a 3D graph. It shows the temporal evolution of the height profile for $Q = 5$ wooden pegs. The evolution of the maximum heap height is plotted in figure 6, top right. In addition, the total volume of the granular bed was recorded. It is discussed in the [appendix](#). The total volume allows to estimate the



changes of the mean packing fraction of the material during shearing. However, one has to keep in mind that this packing fraction is spatially inhomogeneous. In most materials the density mainly drops in the shear zone.

The heap formation takes approximately 20 revolutions of the bottom disk. Comparing this with the above determined velocity of tracer pegs, this corresponds to a period in which individual grains perform roughly one fourth to one third of a full secondary flow convection roll.

The initial increase of the granular bed volume is approximately one order of magnitude faster, Reynold's dilatancy is responsible for a quick dilation of the mean packing fraction. After approximately one full rotation of the disk, the maximum volume is reached. After that, partial alignment of the pegs (see, e. g. [21, 24, 25]) reduces the volume again.

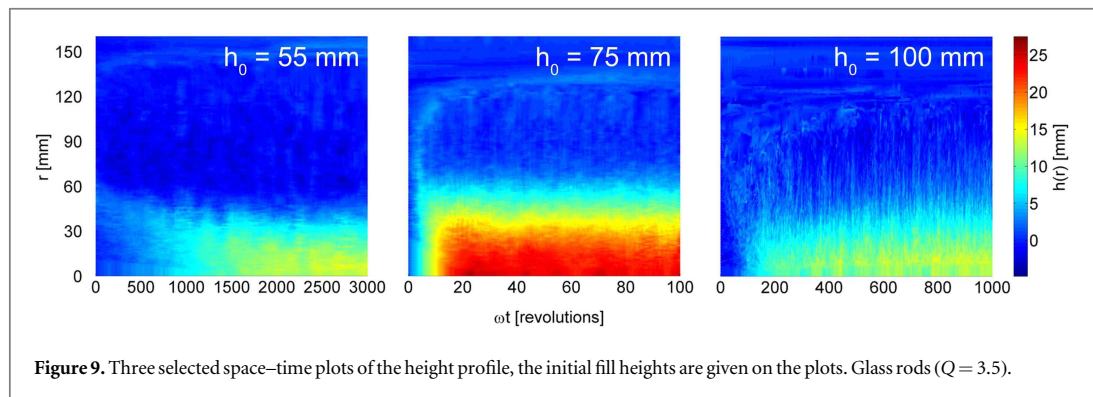
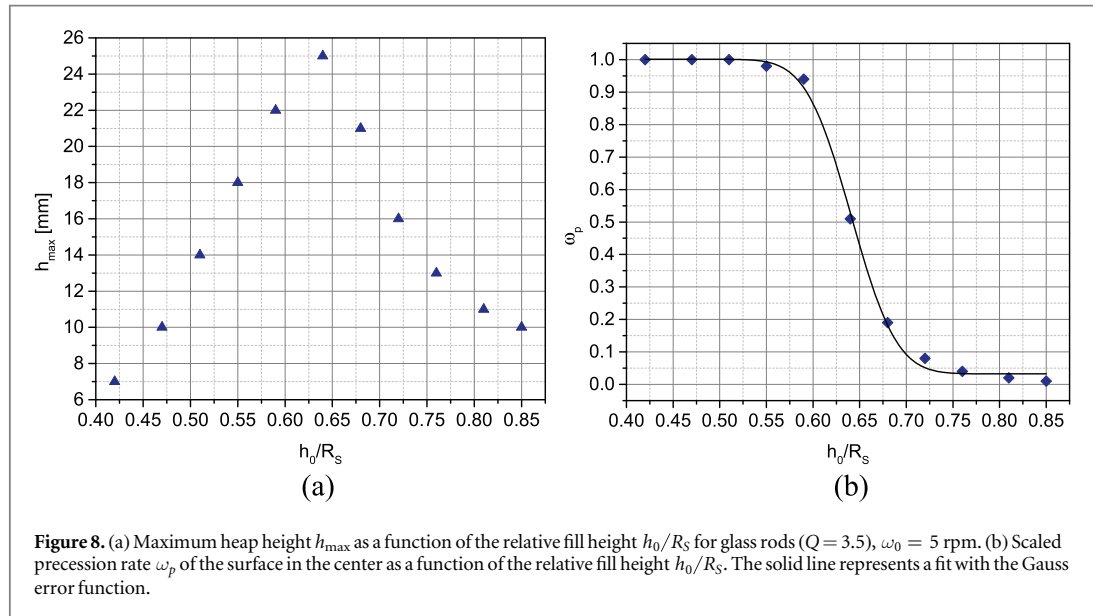
There exists a strong fill height dependence of the heap height. Roughly speaking, the heap formation is most pronounced when the shear zone is bent inwards but still reaches the granular surface. Then, the rotation rate of the granular surface in the container center is intermediate between zero and the rotation rate of the bottom plate. The transition between these two regimes was studied first by Dijkstra and van Hecke [15] and estimated to take place at $h_0/R_s \approx 0.65$.

The $Q = 3.3$ wooden pegs exhibit a much lower tendency to form heaps. The shortest $Q = 2$ pegs did not show any heaping at all. We assume that the anisotropy of these cylinders is too small to initiate spontaneous heaping, similar to spherical grains. The longest $Q = 8$ pegs also show no tendency to form a heap in our setup. Here, the reason may be the too small ratio of fill height and particle length. Wortel *et al* [1] found heaps also for pasta with aspect ratio of about 14, but in their experiment the ratio of container and grain sizes was substantially larger.

While large pegs are particularly suited for x-ray tomography when one is interested to detect all individual grains in a sample, they are less suited for the optical approach primarily used here. The surface profile is rather rough, it reflects the discrete grainy nature of the sample. Thus, smaller particles are favorable, they form a much smoother surface profile of the granular bed. The two images in the bottom row of figure 6 show the same properties as in the top row of that figure, but for the much smaller glass rods with aspect ratio $Q = 3.5$. These reproduce qualitatively the same features, but provide much smoother contour. The ratio of heap height to grain length to grain width is only 2.4:5:1 for the wooden pegs, but 11:3.5:1 for the glass rods. This results in a much better resolution of the glass rod heap profiles. The most remarkable feature is that the dynamics of heap formation is almost the same as for the much larger wooden pegs, the heap is fully developed after approximately 20 revolutions.

The effect of a reversal of the primary flow direction is seen in figure 7. Immediately after the reversal of the shear, the heap height drops to about one half of its original height, and the volume of the granular bed collapses as well. The volume drop is compensated again within much less than one revolution backward, whereas the heap reappears much slower, within approximately 10–20 rotations of the bottom disk.

The heap formation is sensitive to the granular bed height, as reported earlier [1]. Experimental results for the bed height dependence with $Q = 3.5$ glass rods are shown in figure 8(a). For comparison, the relative rotation rate of the granular surface above the bottom plate is plotted in figure 8(b). Here, ω_p is the rotation rate of the granular surface close to the center, scaled by ω_0 .



The limit $\omega_p = 0$ corresponds to the situation where the shear zone is dome-shaped and does not extend to the surface. When $\omega_p = 1$, the ring-shaped shear zone ends at the top surface. Comparison of both graphs 8(a), (b) evidences that the heap forms fastest and gets largest when $\omega_p \approx 0.5$. But on the other hand, heaping is observed even when ω_p is close to 0 or 1. The heap height decreases towards these two limits, but more importantly, the time scale (number of revolutions) of the formation of the heap grows enormously. We verified this for fill levels where more than thousand rotations were needed to produce a heap. In previous work [1], heaping was found only in the intermediate ω_p range because the experiments were limited to a few dozen rotations for each fill height. Figure 9 shows the space–time plot of the heap formation process for three fill levels. The heap width is roughly comparable in all cases, the heap height changes by a factor of about two, the time scales for heap formation differ by up to two orders of magnitude.

In order to confirm that the heap formation at low and high bed heights is caused by the same mechanism as for $\omega_p \approx 0.5$, and not by dilation, we removed the heap carefully after its full development and verified that the heap reappears when shearing is continued. Figure 10 shows examples of very low and high fill levels, respectively. In both cases, the heap reappeared after removal of the excess material. This can be regarded as solid evidence that the heap is formed by a secondary convective flow process in the container. Note the long time scales for the heap formation dynamics.

The study of oblate shaped grains leads qualitatively to comparable results. We sheared lentils with aspect ratio 0.36 in the same container geometry. The lentils align with their symmetry axis at a small angle towards the shear gradient. The results are presented in figure 11. Both heap height and width, as well as the shear necessary to form the heap, are quantitatively comparable to those of the prolate objects with aspect ratios around 3. Reversal of the shear qualitatively leads to the same phenomena as for prolate grains.

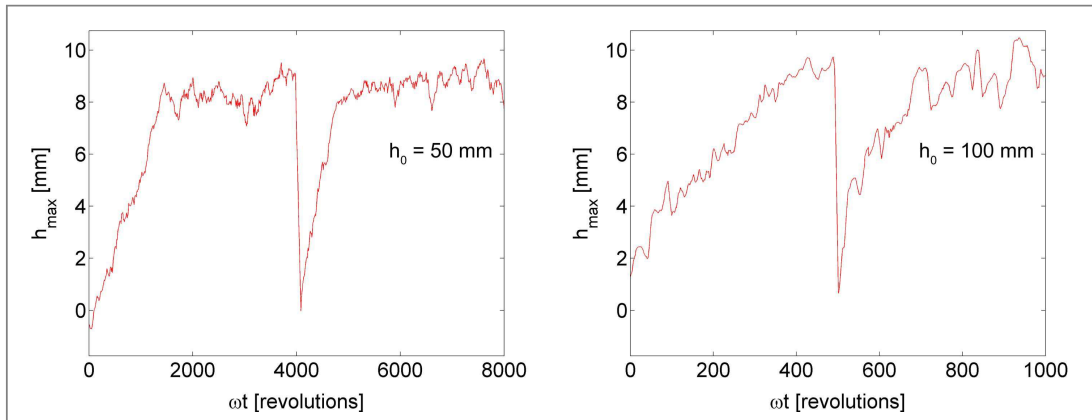


Figure 10. Heap formation from the freshly prepared sample and after removal of the heap (sharp dips in the center of the graphs) in the limits of $\omega_p \approx 1$ (very low fill level), and $\omega_p \approx 0$ (very high fill level). The depth of the granular bed influences the heap height, but more importantly the characteristic times for heap formation are orders of magnitude larger, compared to the optimum fill level.

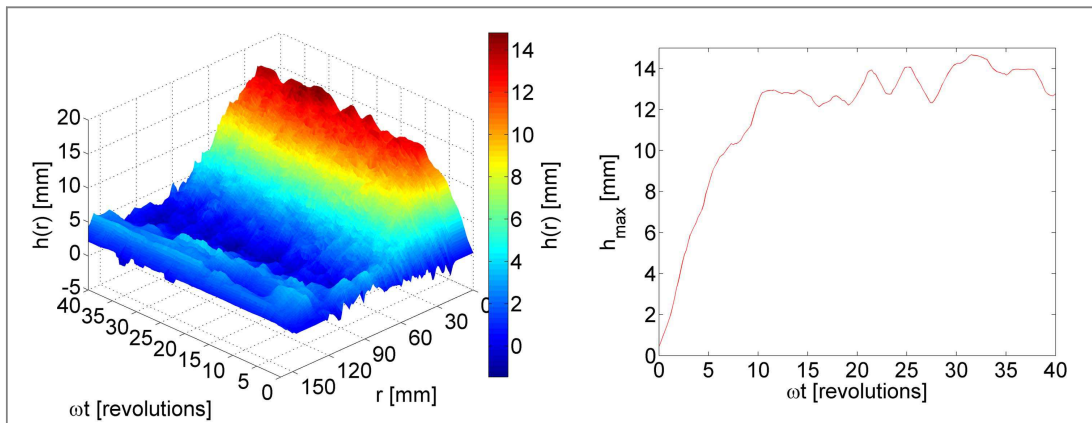


Figure 11. Left: temporal evolution of the height profile for lentils ($Q = 0.36$) at an initial fill height $h_0 = 70$ mm, $\omega_0 = 10$ rpm. Right: maximum height h_{max} of the heap.

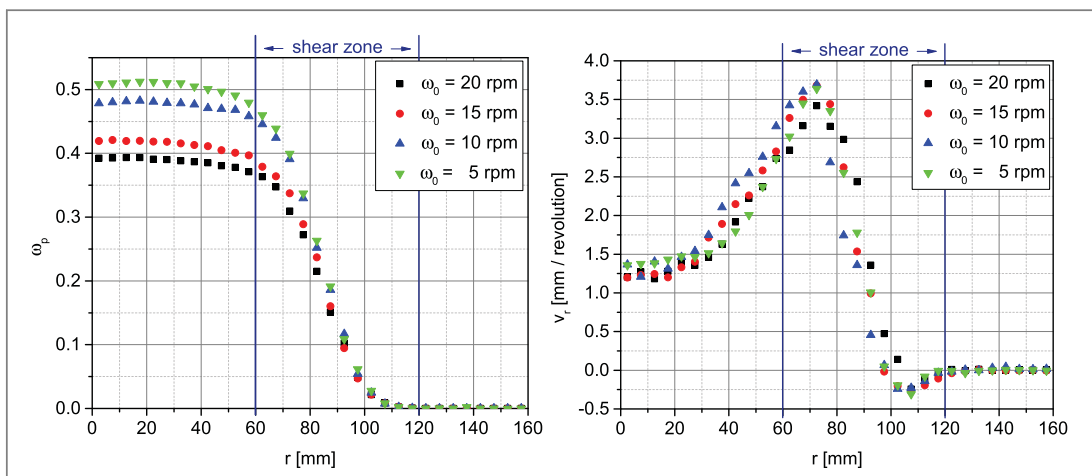
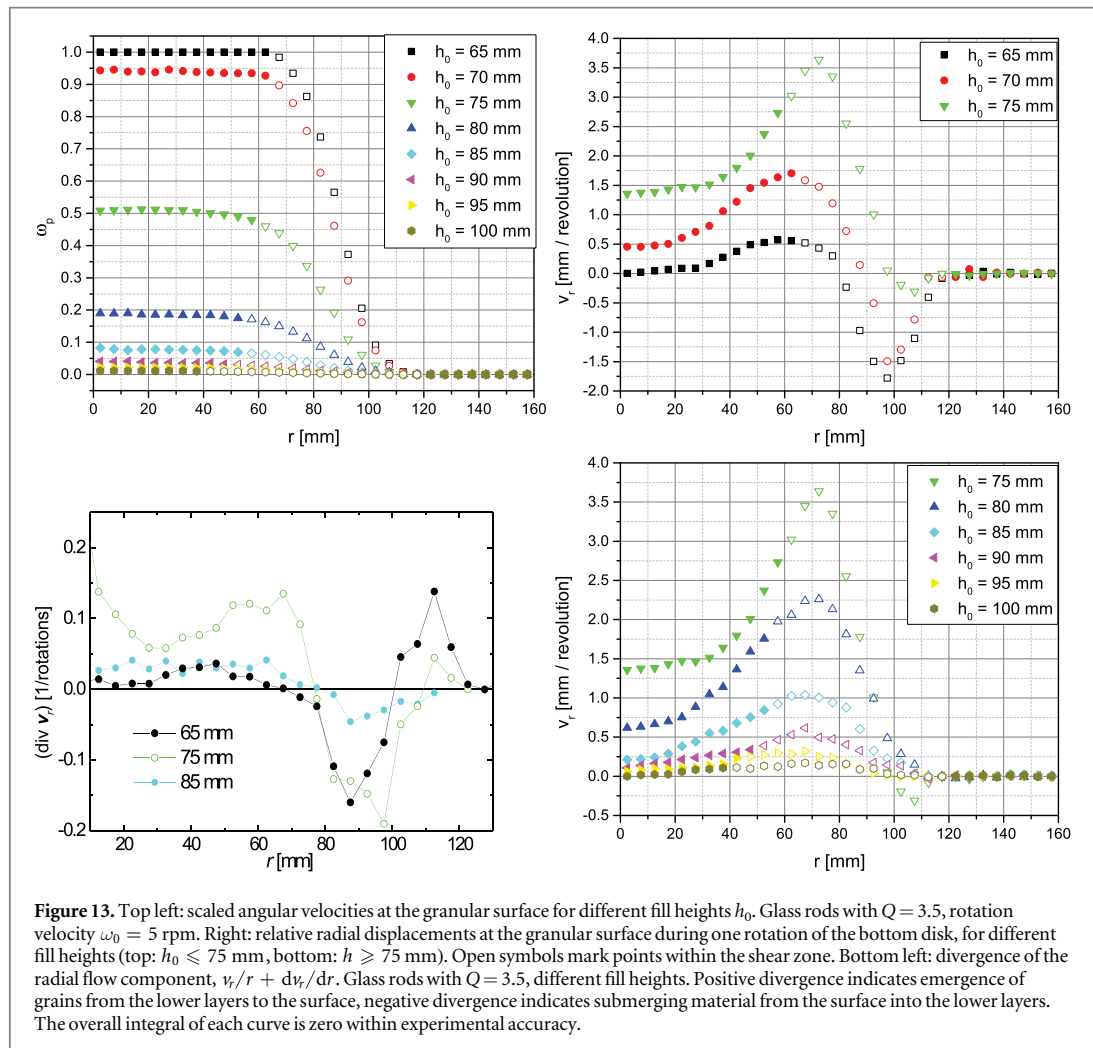


Figure 12. Left: relative angular velocity ω_p at different radial positions of the granular surface, glass rods with $Q = 3.5$ at fill height $h_0 = 75$ mm. Right: relative radial displacements at the granular surface during one rotation of the bottom disk.

3.2. Primary and secondary flows

Velocities of the primary and secondary flows are compared in the following graphs. Figure 12, left, gives the local angular velocity in radial direction on the surface of the granular bed, for different rotation rates ω_0 of the



bottom plate, but fixed bed height h_0 . The fill height chosen corresponds approximately to the maximum heap height. The central plateau of ω_p is above the rotating disk, the steep descent in the shear zone. The reason for the slight decrease of ω_p with higher rotation rates of the bottom disk is presumably some slip occurring in the granular bed.

The radial motion on the granular surface can be taken as a measure for the secondary flow. Figure 12, right, shows the radial velocity. It is practically independent of the bottom disk rotation rate ω_0 . The divergence of the radial component of the flow field is clearly nonzero (see next paragraph). It reflects the emerging of grains in the container center and their submerging in the shear zone. It is also evident that there is an average slight inward motion in the outer regions of the shear zone. This inward motion must be connected with a net outward velocity in the granular bed and thus with a second, very weak convection in the outer part of the shear zone. Figure 13 shows the same quantities as figure 12, but for different fill heights. The radial motion graphs have been split into separate images for better distinction.

The most interesting aspect appears to be that at low fill heights (top right image), the inward velocity in the outer range of the shear zone grows considerably. This indicates that convection in the very shear zone increases, whereas convection above the disk nearly ceases. In cylindrical coordinates (r, θ, z) , the divergence of the flow field $\nabla \mathbf{v}$ consists of three terms

$$\left(\frac{v_r}{r} + \frac{dv_r}{dr} \right) + \frac{1}{r} \frac{dv_\theta}{d\theta} + \frac{dv_z}{dz}$$

which must sum up to zero in the stationary state to satisfy the continuum equation, provided the packing density can be assumed constant and uniform. Since the tangential component v_θ is constant, the first term in parentheses is a measure for the flow of grains into the bulk or out of the bulk to the surface. This term, the divergence of the radial flow field, is plotted in figure 13, bottom left, for low, optimal and high fill heights h_0 . At the optimum fill height 75 mm, the material rises above the bottom plate, and submerges in the shear zone. In

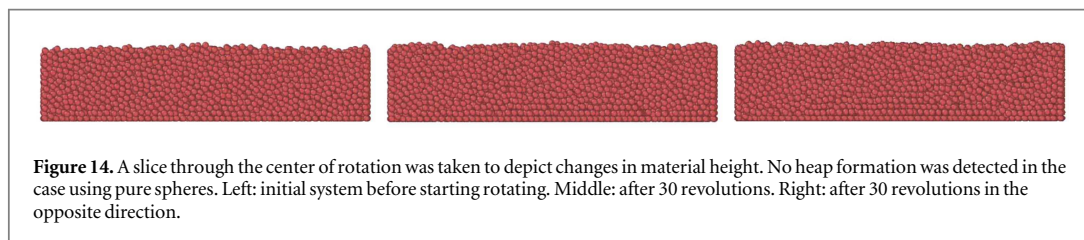


Figure 14. A slice through the center of rotation was taken to depict changes in material height. No heap formation was detected in the case using pure spheres. Left: initial system before starting rotating. Middle: after 30 revolutions. Right: after 30 revolutions in the opposite direction.

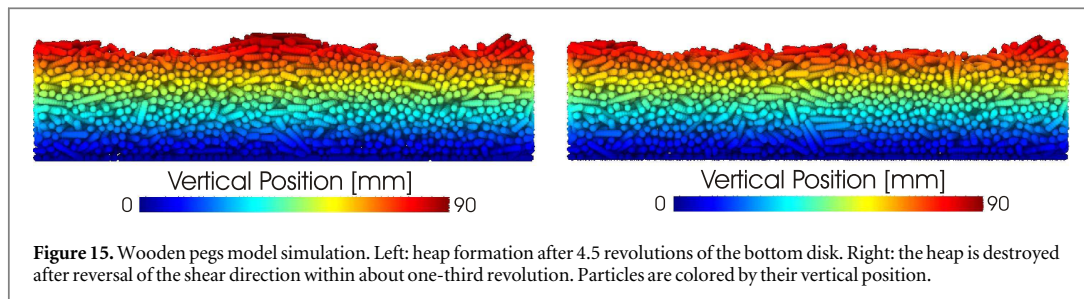


Figure 15. Wooden pegs model simulation. Left: heap formation after 4.5 revolutions of the bottom disk. Right: the heap is destroyed after reversal of the shear direction within about one-third revolution. Particles are colored by their vertical position.

contrast, at low fill heights only little material rises above the central disk, the main share of grains emerges in the outer section of the shear zone and submerges in the inner part of it. The reason for the latter behavior is not clear yet, it must be related either to the curvature of the shear zone or to its inward inclination.

4. Numerical results

For the peas model, 30 revolutions were simulated in each direction with a rotational velocity of 4.7 rpm and a fill height $h_0 = 75$ mm. A slice (depth of 50 mm) normal to the x -axis of our coordinate system passing through the center of rotation of the shearing cylinder was taken, it is displayed in figure 14. No heap formation was found in this numerical simulation using purely spherical particles.

The wooden pegs model was simulated with a rotational velocity of 3.0 rpm and a fill height $h_0 = 75$ mm. Results from our numerical simulations show the formation of a granular heap in the central zone of the mixer after about 4.5 revolutions (see figure 15 left), which is in nice agreement with the experimental data. In addition, a region with negative elevation (with respect to the initial height) could be seen in the zone between the borders (static) and the central zone (heap formation). A similar region can be observed in the experiments, as detailed in figure 6 top left.

When the rotation direction was reversed in our numerical simulations, a collapse of the central heap was observed after one-third revolution in the opposite direction. This is demonstrated in figure 15 right.

The temporal evolution of the height profile for the wooden pegs was obtained using the same methodology as in the experiments. This temporal evolution can be seen in figure 16 left. The moment when the rotation was reversed is indicated in the graph; it is followed by a steep reduction in the heap height.

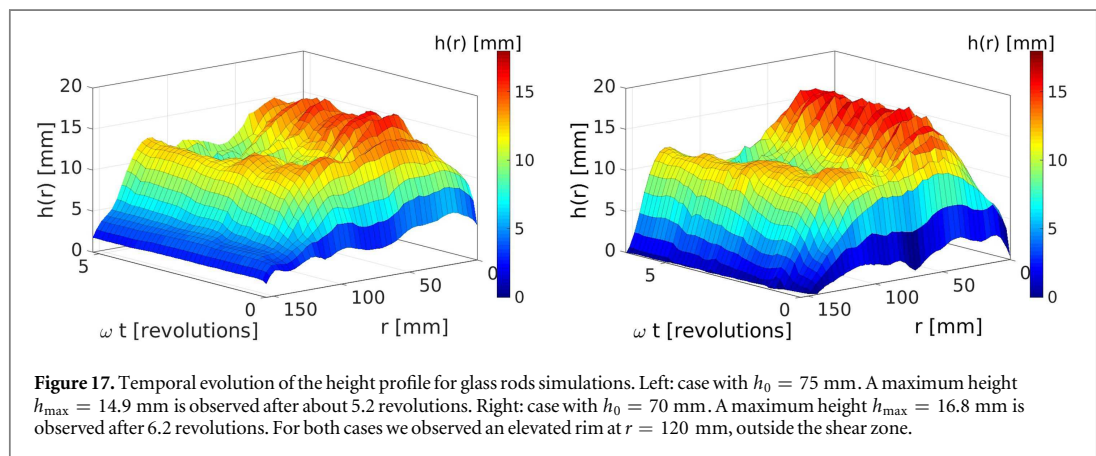
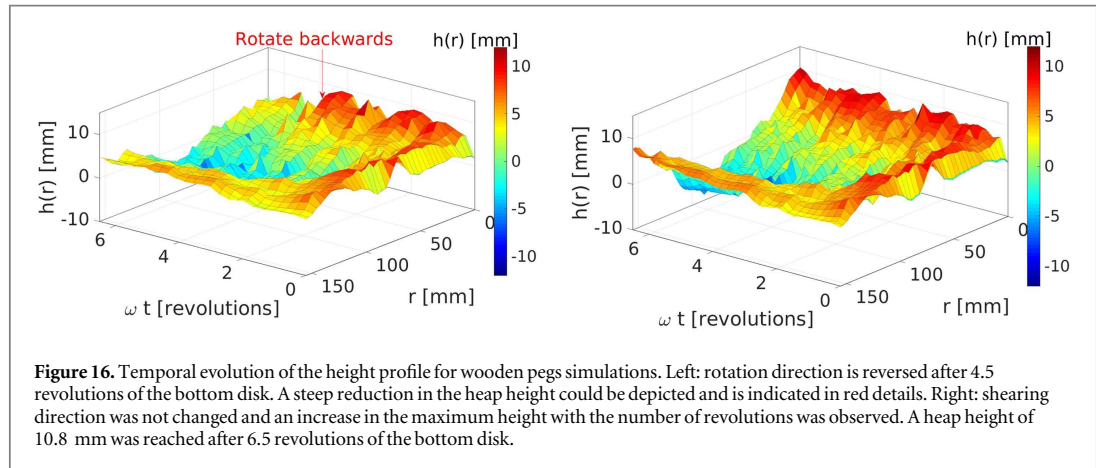
For comparison, the wooden peg model was simulated for a longer time without reversing the rotation (see figure 16, right). In this case, a continuous increase of the maximum heap height is observed. The simulation was stopped before the asymptotic stationary heap height was reached.

The temporal evolution of the height profile was also simulated with the glass rods model. Results for the glass rods with $h_0 = 75$ mm can be seen in figure 17 left. They exhibit a similar profile as the experimental results. Also, the maximum height (16.8 mm) approximates the experimental measurements.

In addition to the central granular heap, numerical simulations also captured the formation of a secondary, smaller heap at a radial distance of 120 mm from the center of rotation. Although a shallow elevation seem to be indicated also in some experimental runs, this feature is clearly over-exaggerated by the simulations.

A further simulation of glass rods was performed for an initial height $h_0 = 70$ mm. The temporal evolution of the height profile is seen in figure 17 right. Similarly to the case with $h_0 = 75$ mm, the maximum heap height depicted approximates that of the experiment. A secondary heap (rim) was also formed.

One detail of the simulations is unclear at first glance: the granular bed forms a rim at the container wall for wooden pegs, but a depletion near the outer wall for glass rods. We think this is caused by the influence of the external container wall, which has frictional interaction with particles in the numerical simulations, in combination with the grain size versus container dimension. The rim is located farther outward for the larger wooden pegs, so that it is formed near the container wall. For the smaller glass rods, the rim appears closer to the



shear zone, so that the profile decays toward the container walls. We note that a similar characteristics is indicated in the experiments (figure 6), although at a considerably smaller magnitude.

5. Conclusions and summary

The experiments show that heap formation in a circularly sheared granular material can be observed for both prolate and oblate axially symmetric particles. The heap heights and heap formation rates for prolate and oblate grains with comparable axes ratios ($Q = 3.5$, $Q = 0.36$) are of the same order of magnitude. After start of shearing, the volume change due to dilation occurs much faster than the heaping. Heap formation has a negligible influence on the relative volume of the granular bed, i. e. it represents basically a redistribution of grains in the container, leaving the mean packing density unchanged.

We find the heaping effect over a considerable range of container fill heights. This includes the cases where the shear zone is nearly vertical, ring-shaped ($h_0 = 65$ mm), and where the shear zone forms a closed dome below the granular bed surface ($h_0 = 100$ mm). In both cases, the rates of heap formation are considerably slower (up to several orders of magnitude) than for the optimum fill height. The heap heights are lower but at least of a comparable order of magnitude as the optimal heap.

Evidently there is a strong quantitative and qualitative influence of the fill height on the secondary flow. When the fill height increases above the optimum 75 mm ($h_0/R_S = 0.635$), the shear zone closes in above the rotating disk, and both the radial flow and the divergence of the radial flow field decrease globally. The heap height consequently drops with the rate of the upward flow in the center. However, when the container fill height is lowered below the optimum 75 mm, a substantial divergence of the radial flow field remains (figure 13). Yet the structure of the radial flow field changes, indicating that the convective flow transforms qualitatively. The secondary flow restricts to the shear zone, and the convection above the bottom disk ceases. It is not possible to give a clear explanation for this change. The divergence of the radial flow in the 65 mm bed is quantitatively comparable to that for the optimum bed height. This indicates that the vertical convection velocity is of the same

order of magnitude. The integral of each graph in figure 13 is zero within experimental accuracy, which is confirmation that the evaluation method is correct (the amount of grains entering and leaving the surface layer averages out).

In order to trace the origin of the heaping effect, we also investigated two types of spherical grains, monodisperse perfect spheres and slightly ($\approx 10\%$) polydisperse imperfect spheres. We do not find any heaping effect with any of these materials. Their granular bed surface remains flat, no secondary flow is observed by optical analysis of the surface.

It is evident that the secondary flow of shape-anisotropic particles out of the shear zone towards the center of the cell is the source of the heaping phenomenon. But still, the detailed mechanism of this flow process needs to be identified. Symmetry arguments were applied [1] to explain the qualitative behavior of heaping under shear reversal. They cannot explain why the permanent flow out of the shear zone is triggered at all, and why the asymmetry between the inner and outer region exists. The present experiments reveal that secondary flow and heaping are maximal when the shear zone bends towards the center of the container but does not form a closed dome. Nevertheless, heaping is also found when the inner part of the granular bed rotates rigidly with the bottom disk, and when the inner part is at rest with the outer container. Critical limits for the granular bed height were not found, the experiments rather indicate a rapid and continuous growth of the time scales with the granular bed height increasingly differing from the optimal value.

Our numerical simulations correctly captured the absence of heap formation for the case of purely spherical particles. This is in agreement with experimental measurements using peas and airsoft bullets. For the wooden pegs model there was a clear heap formation after 4.5 revolutions, and a subsequent collapse when the rotation direction of the bottom plate was reversed. Also, the simulation allowed to run until 6.5 revolutions without changing the direction of the bottom plate reproduced an increase in the maximum heap height with the number of revolutions. In addition to that, a depression region above the shear zone between the peripheral (static) and the heap formation zone was captured. This was also observed in experimental measurements.

For the glass rods case with $h_0 = 75$ mm there was a good agreement both regarding the heap formation dynamics and the maximum heap height. The numerical model also depicted the formation of a secondary, less elevated rim outwards beyond the shear zone (about 120 mm from the center of rotation). However, these numerical results differ from the experimental observations, where only a very shallow elevation may be indicated. In addition to that, the height of the heap fluctuated considerably in the numerical simulations. Maximum elevations of 14.9 mm ($h_0 = 75$ mm case) and 16.8 mm ($h_0 = 70$ mm case) were depicted in our numerical simulations of the glass rods.

There is still room for improvement in the numerical model. A better description of the particle geometry could be achieved by adding more spheres to approach the desired shapes. This is expected to improve the quality and relevance of our numerical results, as the experiment indicates the sensitivity of the effect to the particle shape. Moreover, a calibration process of DEM frictional parameters could improve our numerical results quantitatively. However, even with the present approximations it has been demonstrated that the simulated dynamics reflects most of the experimental findings even quantitatively. Further simulations will allow to study the influences of the container size to particle size ratio and other details, in order to predict which interesting parameter ranges should be explored in future experiments. A particularly interesting aspect is the extension of the aspect ratio far beyond 10, an interesting range for technical applications such as the handling of needles or nails.

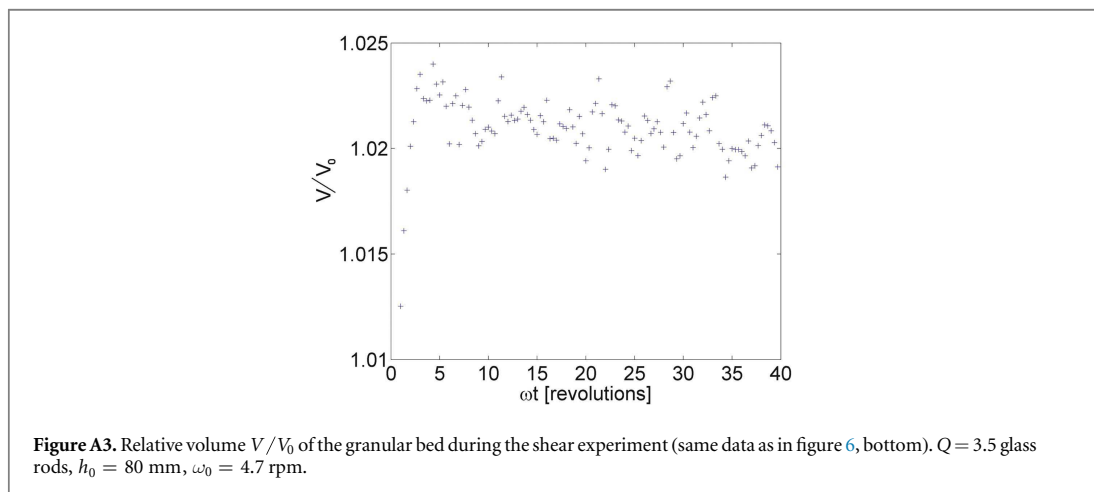
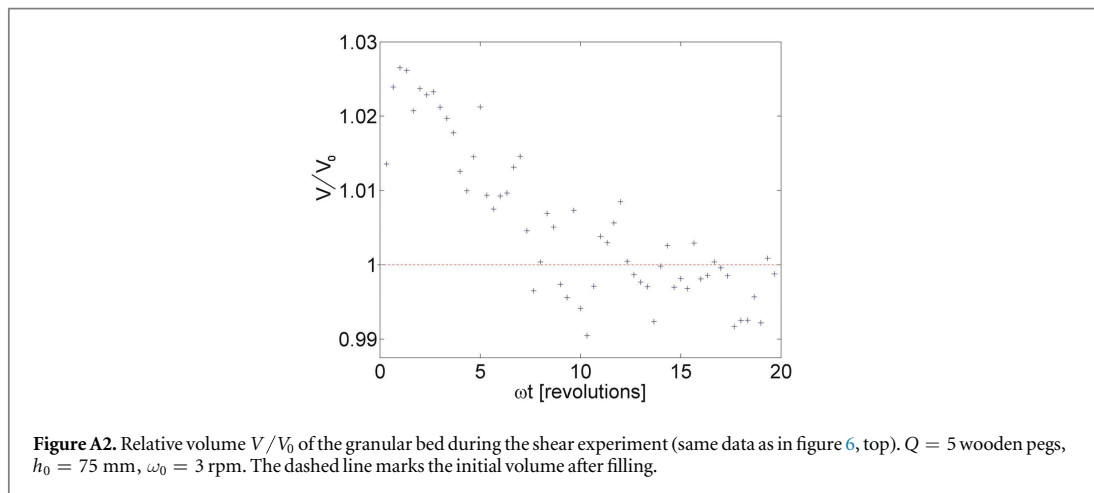
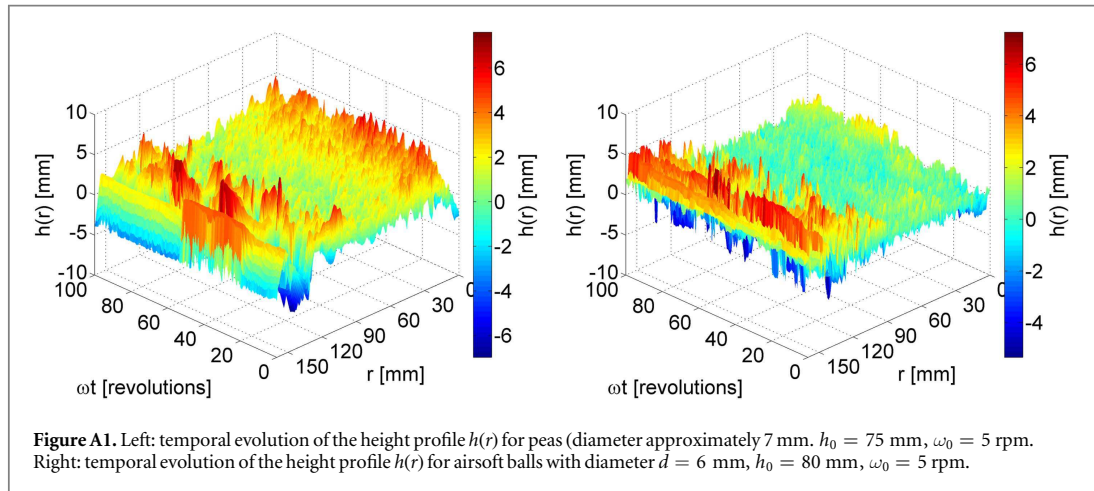
Acknowledgments

Financial support from the DAAD/MÖB researcher exchange program (Grants No. 57141022/64975), from DFG (Grant STA 425/38), and from the Hungarian Scientific Research Fund (Grant No. OTKA NN 107737) is acknowledged. We thank the German Research Foundation (DFG) for funding through the Cluster of Excellence 'Engineering of Advanced Materials', ZISC, FPS and the Collaborative Research Center SFB814. The authors are indebted to Torsten Trittel for technical assistance and helpful comments.

Appendix

A.1 Results for isotropic particles

For a comparison, experiments have been performed with isotropic (sphere-shaped) grains. These do neither show heaping, nor a measurable secondary flow. Figure A1, left, shows the surface of the granular bed for peas. There is only a slight depression of the shear zone, which occurs within the first rotation of the bottom disk, the height difference is well below the particle diameter. Near the outer container walls, this height graph is not representative because the particle arrangement is practically stationary, except for slow creeping motions. The



airsoft balls show a global depression of the granular bed (figure A1, right) because they pack more efficiently when they are sheared [21]. The granular bed remains completely flat during shearing. A long-term observation of grains at the surface show no net radial motion of grains in any of these two cases.

A.2 Dilation

Two observations evidence that the heap formation is not related to dilation of the sheared material. The first one is the observation that the heap reappears when the material from the heap has been completely removed

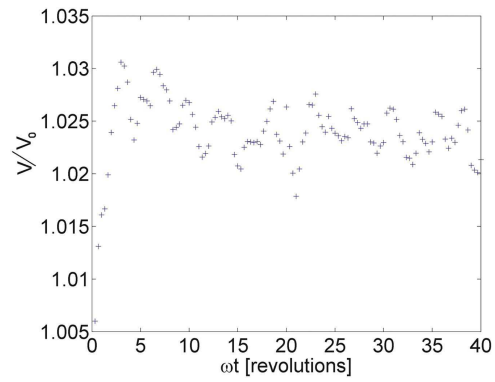


Figure A4. Relative volume V/V_0 of the granular bed during the shear experiment (same data as in figure 11). $Q = 0.36$ lentils, $h_0 = 70$ mm, $\omega_0 = 10$ rpm.

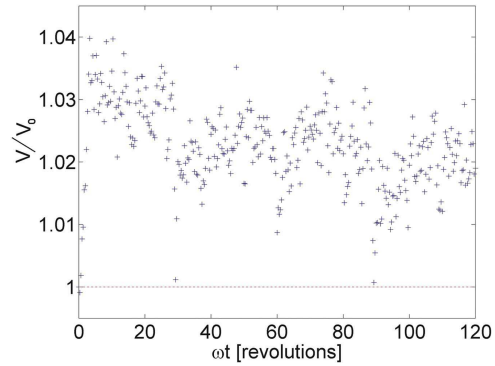


Figure A5. Relative volume V/V_0 of the granular bed during repeated reversal of the shear direction every 30 revolutions (same data as in figure 7). $Q = 3.5$ glass rods, $h_0 = 80$ mm, $\omega_0 = 4.7$ rpm. The dashed line marks the initial volume after filling.

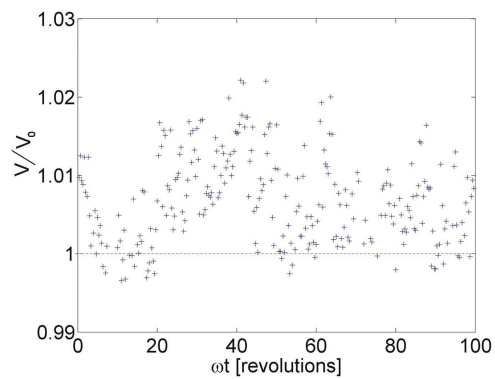


Figure A6. Relative volume V/V_0 for peas (same experiment as in figure 18, left), $h_0 = 75$ mm, $\omega_0 = 5$ rpm. The dashed line marks the initial volume.

(see e. g. figures 10). The second one is the difference in the time scales for dilation of the granular volume and heap formation. As shown in section 3.1, the heap typically appears after a dozen rotations to several hundred rotations of the bottom plate, depending on the fill height. The increase of the initial volume of the granular bed takes place within one revolution or even less. Figures A2–A4 show the measured relative volumes, scaled by the original fill volume, for different prolate (pegs, glass rods) and oblate (lentils) samples. One can see the initial

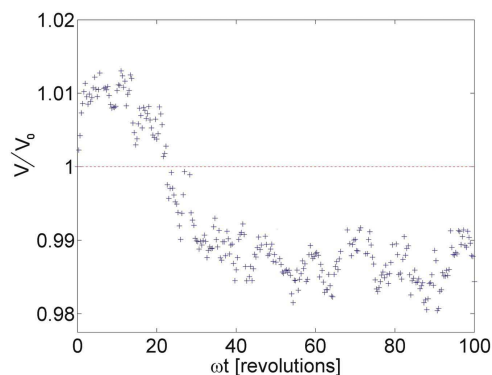


Figure A7. Relative volume V/V_0 of airsoft balls (same data as in figure 18, right), $h_0 = 80$ mm, $\omega_0 = 5$ rpm. The dashed line marks the initial volume.

volume increase by a few (two to four) percent in all these samples. After that, a slow decay of the granular volume takes place. The volume reduces by nearly one percent but does not reach the original volume again, except for the $Q = 5$ wooden pegs which compactify again to roughly the original volume.

When the shear direction of a sample is reversed, the volume quickly drops to nearly the original value, but then it grows again with roughly the same rate as from the initial disordered state. This is shown for the $Q = 3.5$ glass rods in figure A5. Again, these processes are much faster than the drop and the recovery of the heap height.

The isotropic materials also show the initial volume expansion. Reynolds dilatancy changes the global volume occupied by the peas (figure A6) within fractions of a full rotation of the bottom disk by approximately 1%. As there is no alignment process in the peas sample, the volume stays roughly constant afterwards. The measured volume effect is an average of all parts of the container, thus it is not representative for the dilation in the shear zone. There, the decrease in packing fraction is much larger. For the airsoft balls (figure A7), crystallization leads to a reduction of the granular bed volume after a fast initial expansion by Reynolds dilatancy (see Wegner et al [21]).

References

- [1] Wortel G, Börzsönyi T, Somfai E, Wegner S, Szabó B, Stannarius R and van Hecke M 2015 *Soft Matter* **11** 2570–6
- [2] van Hecke M 2010 *J. Phys. Cond. Matter* **22** 033101
- [3] Torquato S and Stillinger F H 2010 *Rev. Mod. Phys.* **82** 2633
- [4] Luding S 2016 *Nat. Phys.* **12** 531
- [5] Zuriguel I, Janda A, Garcimartin A, Lozano C, Arevalo R and Maza D 2011 *Phys. Rev. Lett.* **107** 278001
- [6] Thomas C C and Durian D J 2015 *Phys. Rev. Lett.* **114** 178001
- [7] Börzsönyi T, Szabó B, Törös G, Wegner S, Török J, Somfai E, Bien T and Stannarius R 2012 *Phys. Rev. Lett.* **108** 228302
- [8] Börzsönyi T and Stannarius R 2013 *Soft Matter* **9** 7401
- [9] Duran J 2000 *Sands, Powders, and Grains* (New York: Springer)
- [10] Jaeger H M, Nagel S R and Behringer R P 1996 *Rev. Mod. Phys.* **68** 1259–73
- [11] Aranson I S and Tsimring L S 2006 *Rev. Mod. Phys.* **78** 641–92
- [12] Börzsönyi T and Stannarius R 2013 *Soft Matter* **9** 7401–18
- [13] Fenistein D and van Hecke M 2003 *Nature* **425** 256
- [14] Fenistein D, van de Meent J W and van Hecke M 2004 *Phys. Rev. Lett.* **92** 094301
- [15] Dijkstra J A and van Hecke M 2010 *Soft Matter* **6** 2901–7
- [16] Woldhuis E, Tighe B and van Saarloos W 2009 *Eur. Phys. J. E* **28** 73
- [17] Moosavi R, Shaebani M R, Maleki M, Török J, Wolf D E and Losert W 2013 *Phys. Rev. Lett.* **111** 148301
- [18] Singh A, Magnanimo V, Saitoh K and Luding S 2014 *Phys. Rev. E* **90** 022202
- [19] Sakaie K, Fenistein D, Carroll T J, van Hecke M and Umbanhowar P 2008 *Europhys. Lett.* **84** 38001
- [20] Slotterback S, Mailman M, Ronaszegi K, van Hecke M, Girvan M and Losert W 2012 *Phys. Rev. E* **85** 021309
- [21] Wegner S, Stannarius R, Boese A, Rose G, Szabó B, Somfai E and Börzsönyi T 2014 *Soft Matter* **10** 5157–67
- [22] Hill K M and Fan Y 2008 *Phys. Rev. Lett.* **101** 088001
- [23] Fan Y and Hill K M 2010 *Phys. Rev. E* **81** 041303
- [24] Börzsönyi T, Szabó B, Wegner S, Harth K, Török J, Somfai E, Bien T and Stannarius R 2012 *Phys. Rev. E* **86** 051304
- [25] Wegner S, Börzsönyi T, Bien T, Rose G and Stannarius R 2012 *Soft Matter* **8** 10950–8
- [26] Nichol K and van Hecke M 2012 *Phys. Rev. E* **85** 061309
- [27] Gladky A and Schwarze R 2014 *Granular Matter* **16** 911
- [28] Harrington M, Weijs J H and Losert W 2013 *Phys. Rev. Lett.* **111** 078001
- [29] Murdoch N, Rozitis B, Nordstrom K, Green S F, Michel P, de Lophem T L and Losert W 2013 *Phys. Rev. Lett.* **110** 018307
- [30] Cundall P A and Strack D L 1979 *Geotechnique* **1** 47
- [31] Parteli E J and Pöschel T 2016 *Powder Technol.* **288** 96

- [32] Pöschel T and Schwager T 2005 *Computational Granular Dynamics* (Berlin: Springer)
- [33] Brilliantov N V, Spahn F, Hertzsch J M and Pöschel T 1996 *Phys. Rev. E* **53** 5382
- [34] Renzo A D and Maio F P D 2004 *Chem. Eng. Sci.* **59** 525–41
- [35] Kloss C, Goniva C, Hager A, Amberger S and Pirker S 2010 *Prog. Comput. Fluid Dyn. Int. J* **12** 140
- [36] Pei C, Wu C Y and Adams M 2015 *Powder Technol.* **285** 110–22
- [37] Paulick M, Morgener M and Kwade A 2015 *Powder Technol.* **283** 66–76